A Monte Carlo Simulation for the Effect of Compression on an Amorphous Polyethylene Melt in Very Thin Confined Geometry

Jee Hwan Jang and Wayne L. Mattice*

Institute of Polymer Science, University of Akron, Akron, Ohio 44325-3909

Received September 21, 1999; Revised Manuscript Received December 14, 1999

ABSTRACT: The effect of compression on a melt composed of 20 chains of C_{120} polyethylene between two impenetrable solid walls has been studied by a Monte Carlo simulation on a high coordination lattice. The compression is controlled by changing the wall separation between two plates in the confined geometry from $\sim 3R_g$ to $\sim 2R_g$, which produced the overall densities ranging from 0.70 to 0.95 g/cm^3. The density near the walls increases with the compression, which is attributed to an increase of the trans conformation. The effect of the local conformational change near the walls is delivered into the middle region with an oscillation of the bead density profile and an increase of the gauche conformation. For the molecular shape, anisotropy is observed in the whole region of the confined geometry, and the extent of the anisotropy is larger near the interfacial area. The more ordered structure at small scale is observed at the higher compression and the lower temperature. The short time center-of-mass diffusivity along the direction parallel to the wall is much more suppressed than the perpendicular component with the compression, though the parallel component is always larger than the normal component at a specific compression.

Introduction

Polymer melts between two plates have attracted many simulation works and theoretical considerations. Despite its practical importance in areas such as lubrication, extrusion, and membranes, few experimental works at the molecular level of study have been performed due to the difficulty in their design, which make the simulation works more important. The confinement can be simply introduced in the simulation by placing the polymer melts between two parallel hard walls. Most of the works[1−6] have used the Monte Carlo technique due to the long time and length scales in the system of interest, which cannot be easily explored by a fully atomistic simulation. Fully atomistic simulations have been performed for chains, such as *n*-tridecane,[7] that are not too long. Some findings in the works are in common.[8] The existence of the interfacial region near the solid wall was observed, and the width of the interface was shown to have the length scale[1,2] of $\sim 2R_g$, where R_g is the radius of gyration of the single chain in the bulk state. In the interfacial region, chains were observed to have a tendency to orient toward the wall. Beyond the interfacial region is an isotropic inner region which is not perturbed by the interface.

Even though those works gave insights into the chain properties in the confined geometry, much of the detailed knowledge at the molecular or atomic level for systems with long chains was sacrificed by the coarse grained nature. The coarse graining produced a chain of beads, but detail smaller than the beads, which should be responsible for the local conformation, was ignored. For that reason, the choice of the macroscopic simulation parameter like density was quite arbitrary. In those coarse grained models, the density in the confined system was chosen to be a value that is comparable with a molten state of a model polymer[1−2,4,5] or to provide a full occupancy in the simulated lattice.[3,6] Those densities were not necessarily the same as the real density, and do not need to represent a real system either, because the concerns of those studies were mainly focused on comparing the behavior of the confined system to the bulk system.

Our concern in this study is to see how compression affects the behavior of the very thin confined system. The thickness of the confined system varies from $\sim 3R_g$ to $\sim 2R_g$, which is thin enough that the two interfacial regions near the two walls can overlap. The compressed system can be simply achieved by changing the separation between two impenetrable walls with other variables unchanged, which results in a change of the density in the confined geometry. In a recently developed lattice model[9−11] the density in the middle of a free-standing thin film[12] is decided by the system during the simulation through the specially devised Hamiltonian. This model possesses two energy contributions: the short-range interaction[9] from the rotational isomeric state model[13] for unperturbed polymers and the long-range interaction[10] from the Lennard-Jones potential of pairs of small molecules in the gaseous state. The use of the Hamiltonian has been validated in the previous studies for freely standing films[12] and thin films[14] attached at an attractive solid wall, producing reasonable density profiles with good agreement to experimental observations. In addition, the energetics[12] represented by the cohesive energy and the surface energy was found to be in good agreement with experiment. In this paper, we present findings about the effect of compression when the compression is simply implemented in our simulation by changing the wall separation.

Computations

The lattice structure, the energetics, and the moves for the present simulation are described in detail elsewhere.[9−11] The monodisperse melt of 20 chains of $C_{120}H_{242}$ was mapped onto the periodic second nearest diamond lattice (2nnd) at 443 K through the rotational isomeric state (RIS) model. The lattice structure is a coarse grained version of a diamond lattice discarding every second site in the lattice whose bond length is 1.53 Å. The coarse graining produces a distorted cubic unit cell whose step length, *l*, is 2.5 Å, and the angles between any two unit vectors are 60°. For a linear hydrocarbon, each occupied site on the 2nnd lattice

10.1021/ma991605m CCC: $19.00
Published on Web 01/27/2000

represents a $-CH_2CH_2-$ unit. Accordingly, the mapping of each $C_{120}H_{242}$ chain generates 60 beads in our 2nnd lattice. In addition, the mapping requires a condensed version of the conventional RIS model for polyethylene.[15] The rotational isomeric states between i and $i + 2$ beads can be categorized into four groups that are specified by the distances between these two beads.[9] The distances of 5.00, 4.33, 3.53, and 2.50 Å correspond to the local conformations of tt, (tg^+,tg^-,g^+t,g^-t), (g^+g^+,g^-g^-), and (g^+g^-,g^-g^+), respectively. The long-range interaction was put into our simulation as the discrete shell parameters which were obtained by the averaging process[10] of the Meyer function for each shell. This simulation uses the first, the second, and the third shell interaction parameters, which are 14.122, 0.526, and −0.627 kJ/mol, respectively. Those interaction parameters are multiplied by the total numbers of non-nearest-neighbor or next-nearest-neighbor beads in the first, the second, and the third shell around a bead of interest. Only three shell interaction parameters are used for the computational efficiency, implying a cutoff distance of 7.5 Å in the long-range interaction.

The single bead move was employed in the simulation with the restriction that a chain cannot pass through itself, as in a self-avoiding random walk. For the equilibration, 5 million Monte Carlo steps were performed, with one Monte Carlo step defined as the simulation length when every bead has attempted one move, on average. The equilibrated bulk structure was put in the expanded z periodicity in order to generate a freely standing film and relaxed for a further 2 million Monte Carlo steps. Then, two impenetrable solid walls parallel to the xy direction were placed at lattice planes $z = 0$ and $z = H$ after eliminating z directional periodicity with the relaxed freely standing film structure. The separations between the two walls are crucial to control the compression. Five kinds of wall separations, from $H = 11l$ to $H = 15l$, have been used. They correspond to the average densities of 0.95 to 0.70 g/cm^3, respectively. It should be noted that $\sim 10^3$ bar order of pressure is required to compress a polyethylene melt to achieve the highest density based on the dilatometric measurement.[16] These wall separations correspond to the length scale ranging from $\sim 2R_g$ to $\sim 3R_g$. Each confined system was relaxed for 5 million Monte Carlo steps at the increased temperature, 543 K, since the confined geometry was expected to relax slowly. An additional 5 million steps of Monte Carlo simulation have been carried out at 443 and 513 K for each structure. A further 5 million steps at 443 K for each structure and 20 million steps at 513 K for the two highest compressed systems have been done, which is used for data gathering and analysis. All computations were carried out using a R10000 Silicon Graphics workstation, and approximately 150 h CPU time was consumed for the generation, the relaxation, and the data gathering from the 5 million steps of Monte Carlo simulation for each compressed system.

Results and Discussion

Figure 1 shows the comparison of the bead density profiles for the confined systems at 443 K with varying separation, that is, different compression. The density profiles at 513 K (not shown) were almost the same as the profiles at 443 K. The densities were obtained from counting the beads as a function of H and averaging over all configurations. The density of an unperturbed

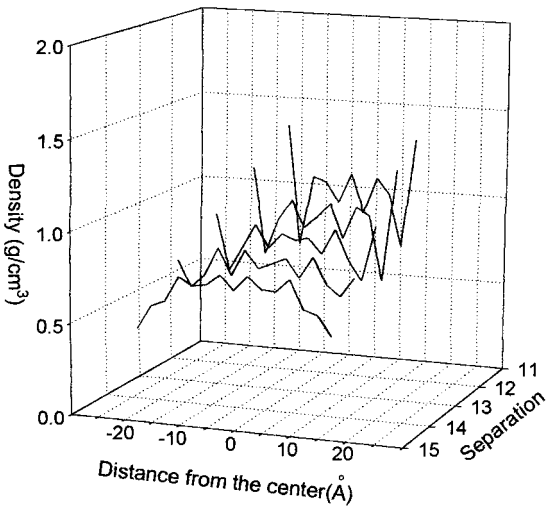

Figure 1. Density profiles of the compressed amorphous polyethylene melts at 443 K in the direction normal to the walls. The compression is varied by the wall separation, H. The separation $H = 11$ corresponds to the highest compression.

melt in our simulation is 0.72−0.74 g/cm^3, obtained from the isotropic middle region in the thicker film simulation.[14] The density of the middle region of the confined system increases with the compression from 0.77 to 0.97 g/cm^3. The density at the solid wall increases with the compression from 0.53 to 1.32 g/cm^3. At the lowest compression in this study, the density profile near the walls retains much of the nature of the interfacial profile of the free surface. The purely repulsive walls cannot affect the thin film if they are located very far away, corresponding to $H = \infty$ in our simulation. Reducing H to a value of 14 still gives a result comparable to this bulklike density. The density adjacent to the solid wall becomes larger than that of the middle region when $H = 13$. Most[1−6] previous Monte Carlo simulations showed an excessive population of the beads at the solid walls when the simulations were carried out at bulklike densities. The bead density at the wall is still smaller than that of the middle region at $H = 14$, as shown in Figure 1. The very thin confined systems with the thickness smaller than $4R_g$ are dealt with in this simulation. Considering the results of others[1,2] for the interfacial width in the confined system, the thickness of at least $4R_g$ is required to observe the isotropic region. Therefore, in our simulation, the two interfacial regions near the two walls overlap together, and the effect near the wall can be communicated into the whole region of the confined system.

Oscillations of the density profiles are observed, and their strength is larger at a higher compression. The second lattice from the wall showed a depletion in bead population, and the depletion is weaker at the fourth layer from the wall. The oscillation of the density profile near the hard wall was observed in other studies and explained by the competition[4] of the packing constraint and the loss in configurational entropy near the flat walls. That rationalization can be applied to our result, and especially, the repulsive interaction of the first and second shell parameters implemented in the long-range interaction plays a role as the excluded-volume interaction. For the very thin compressed system, the cohesive interaction based on long-range attraction would be added to the competition since it affects the density change in the middle region of the confined system.

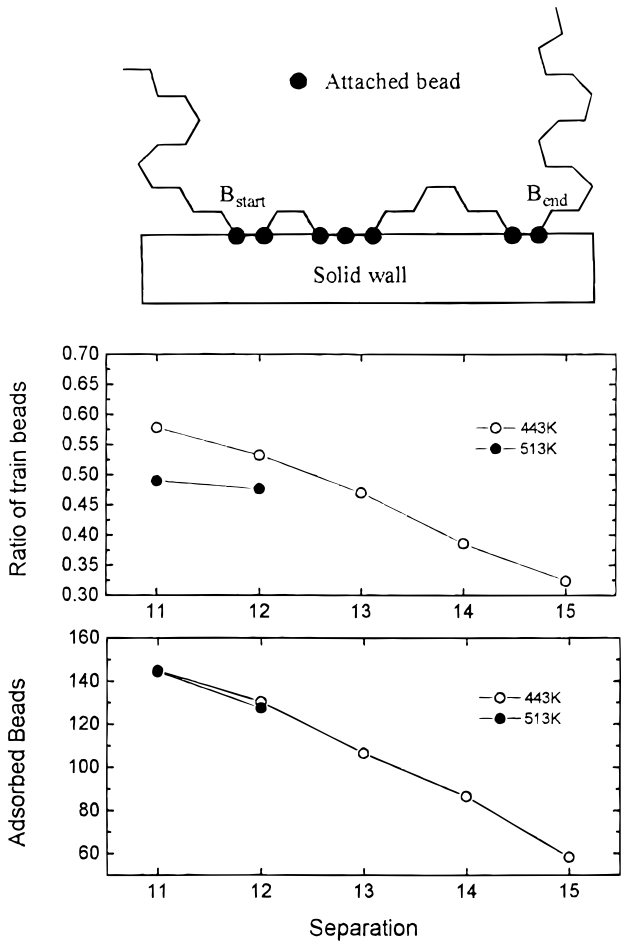

Figure 2. Number of beads attached to the wall (bottom panel). The middle panel represents the ratio of train beads near the wall against wall separation, which is calculated by eq 1. From the top picture, the value 1 for the train bead ratio would indicate that all attached beads in a chain consist of a single train.

The number of beads in direct contact with the solid wall has a nearly linear dependence on the wall separation, as shown in the bottom panel of Figure 2. At the constant temperature, the total number of beads at the solid wall during compression can be considered as proportional to the net pressure exerted by the film on the solid wall, which was pointed out by Kumar et al.[2] Therefore, the force between the two solid walls at constant temperature increases almost linearly with the wall separation or the overall density. At the elevated temperature, there was not much difference in the bead density at the wall compared to that at the lower temperature.

The middle panel of Figure 2 shows the ratio of train beads attached to the solid walls in a chain, which is calculated as

$$\text{ratio of train beads} = \frac{\langle N_{\text{attached}} \rangle}{\langle B_{\text{end}} \rangle - \langle B_{\text{start}} \rangle} \qquad (1)$$

where $\langle B_{\text{end}} \rangle$ is the average of the bead index for the last bead in a chain attached to the wall, $\langle B_{\text{start}} \rangle$ is the average of the bead index for the first bead in a chain attached to the wall, and $\langle N_{\text{attached}} \rangle$ is the average of the total number of the attached beads in the chain. The pictorial representation for B_{start} and B_{end} is depicted at the top of Figure 2.

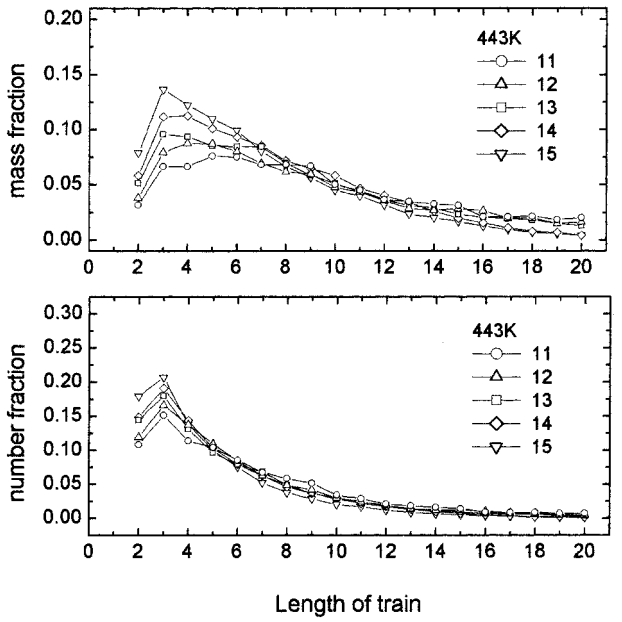

Figure 3. Mass fraction (top) and the number fraction (bottom) against the length of train beads attached to the wall at 443 K.

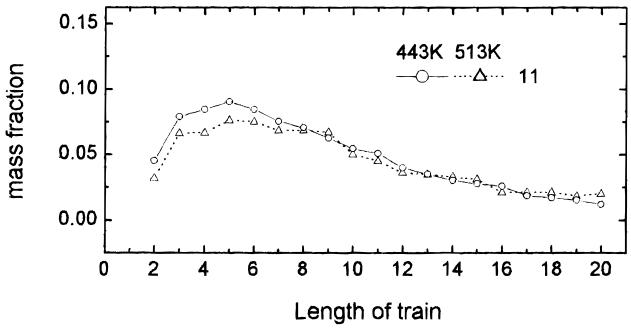

Figure 4. Mass fraction of attached beads at 443 and 513 K as a function of train length in the most highly compressed film.

The ratio of train beads might be the indication of the efficiency of the packing at the walls. The ratio increases with compression, which means that the chains are more easily packed at the walls with compression. From the lower train bead ratio at the higher temperature, less effective packing is expected with increased loop structures near the walls, implying that the chain conformation has a dependence on temperature even though the bead densities at the wall at the two different temperatures are nearly same. The runs of beads to the wall have a length distribution as shown in Figure 3. The train of three beads is the most abundant form in the number distribution. In the mass fraction distribution, the dependence of train length on compression becomes clear, showing that high compression produces more lengthy trains. Here mass fraction is defined as the fraction of all of the mass in trains that is in a train of specified length. The decrease of the ratio of the train beads at the elevated temperature is caused by the less probable population of the short train structure compared to that at the lower temperature. The length of train structures up to six is less probable at the higher temperature, as shown in Figure 4. The dependence of the train structure on compression and temperature is in accordance with the experimental

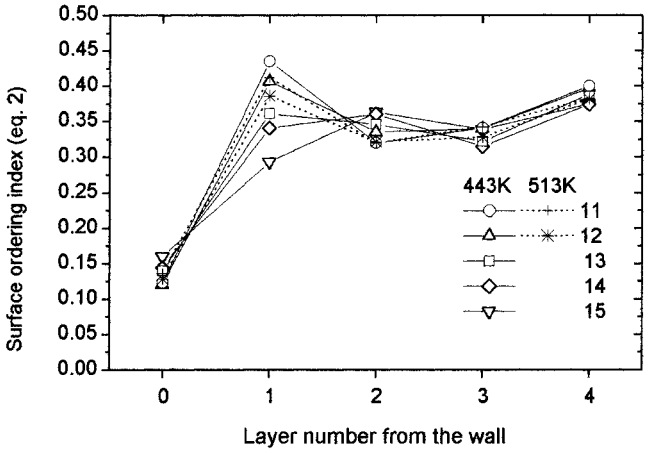

Figure 5. Surface ordering index defined in eq 2, against the layer number. The zero layer is immediately adjacent to the hard walls.

observation[16] that the crystallization temperature increases with pressure.

The increase of the train length does not represent a full range of ordering between chains. To see the large-scale ordering, we used the surface ordering index which was first introduced by Doye et al.[17] Their original form is for two bond vectors on a surface, but our model uses three bond vectors. The modified surface ordering index is defined by

$$\text{surface ordering index} = \sqrt{\frac{9}{6}\sum_{\alpha=1,2,3}\left(\frac{n_\alpha}{n_1+n_2+n_3}-\frac{1}{3}\right)^2} \quad (2)$$

where 1, 2, and 3 are the three possible bond directions on a lattice plane separated by angles of 60° and n_α is the number of bonds in the direction α. Bonds not in the lattice plane are ignored. The index should be 1 if all bonds in a plane are in the same direction and 0 if $n_1 = n_2 = n_3$. The surface ordering index for the five layers starting from the wall is shown in Figure 5. The total numbers of bonds, $n_1 + n_2 + n_3$, for the first five layers from the wall are in the range of 90−250, 60−80, 70−120, 90−120, and 70−80, respectively, varying with compression. Surprisingly, the ordering index at the wall is quite small and even smaller than those of the interior layers. Despite the increase of the train structure, the trains are collapsed onto the wall in a random way. The ordering onto the *xy* dimension is prominent at the second-nearest neighbor to the wall, and the ordering increases with compression and decreases with temperature.

The conformational change and the subsequent bead distribution can be reflected through the energetics. The top, middle, and bottom panels of Figure 6 represent the average energies and the short-range energy from the RIS scheme and long-range energy from the Lennard-Jones potential contributions, respectively. The clear minimum of the long-range interaction is found at $H = 12$ while the short-range interaction shows a maximum at the same separation. The long-range interaction dominates the trend for the total energy. At the higher temperature, the trend in the short-range interaction is not clear, but the total energy has the same trend as at the lower temperature. Because of the attractive nature of the third shell interaction, the long-range interaction decreases with compression until the repulsive first and second shell interactions become prevailing. Previously, the more ordered structure near the wall with higher compression was observed, which indicates a larger trans population. The increase of the total short-range energy with compression indicates a larger population of the gauche conformation exists in the middle region of the confined melts. This also implies that the rearrangement of chain into the trans conformation at a large scale as in high-density polyethylene crystal is hampered in the confined system. As a result, it is expected that the local conformation is a function of distance from the wall in the confinement.

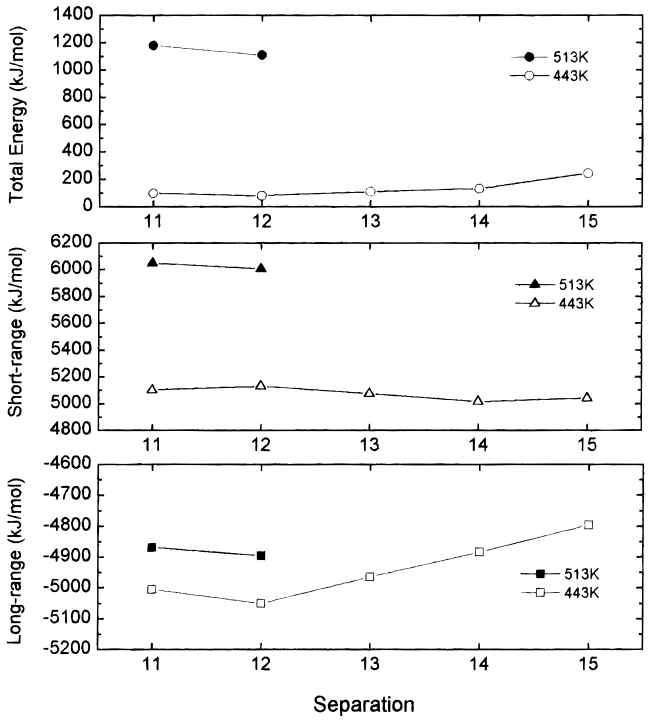

Figure 6. Total energy (top), short-range interaction (middle), and long-range interaction (bottom) against wall separation.

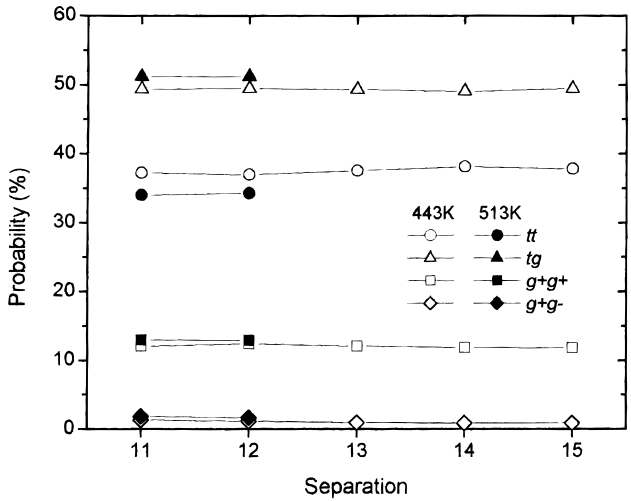

Figure 7. Overall probability for the local conformations corresponding to the rotational isomeric states at two successive C−C bonds.

The overall probabilities for the distinguishable pairs of isomeric states at two consecutive C−C bonds are presented in Figure 7. The population follows the order of (tg^+,tg^-,g^+t,g^-t), tt, (g^+g^+,g^-g^-), and (g^+g^-,g^-g^+). The

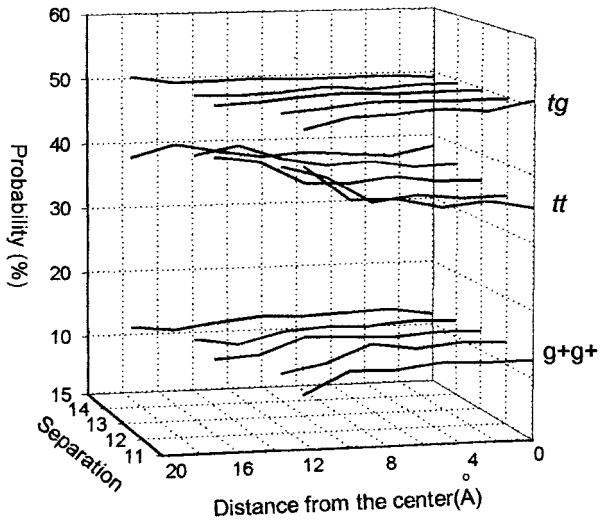

Figure 8. Probability of the local conformation for the compressed polyethylene melt against the distance from the center of the confined system. The *tt*, *tg*, and g^+g indicate *tt*, (tg^+,tg^-,g^+t,g^-t), and (g^+g^+,g^-g^-), respectively. The probability for (g^+g^-,g^-g^+) is not shown due to the small contribution.

populations of (tg^+,tg^-,g^+t,g^-t) and (g^+g^+,g^-g^-) have the same trend as the one of the short-range interaction with compression while the population of *tt* behaves in the reverse way. The population of (g^+g^-,g^-g^+) is very small due to the unfavorable energy state, which is difficult to access even at high compression. The difference in the overall populations with compression is quite small. At the elevated temperature, more gauche conformations are accessible as shown in Figure 7. In Figure 2, we observed the significant increase of the train structure at the walls, which could be attributed to the increase of packing efficiency or the increase of the trans conformation. Despite the excess of trans conformation at the wall, the fact that the overall population throughout the system is quite similar indicates that more gauche conformations are populated in the middle region with compression, giving rise to the very little difference in overall population of each local conformation.

Figure 8 shows the probability of the local conformation against the location of the middle bead in the three-bead segment from the center of the confined system. With compression, the population of the *tt* conformation increases near the walls, but it decreases in the middle of the confined system. The reverse trends are observed for (tg^+,tg^-,g^+t,g^-t) and (g^+g^+,g^-g^-). From this result and Figure 7, the local property can vary much while the macroscopic property is not changed.

The chain dimension was examined by looking at the squared radius of gyration and the parallel and perpendicular components of the radius of gyration of the chain. The averages of the squared radius of gyration, $\langle R_g^2 \rangle$, in the confined systems do not vary much with compression and temperature, as shown in the top panel of Figure 9. The bottom panel shows the parallel component of the radius gyration ($R_{g,xy}$) and the perpendicular component ($R_{g,z}$) against the location of the center of mass of each chain from the center of the confined system. The point at the largest distance from the center, for each value of H, is based on a very small number of observations, due to the low probability of finding the center of mass near the wall. This point is not plotted for $H = 14$. At a specific compression, the

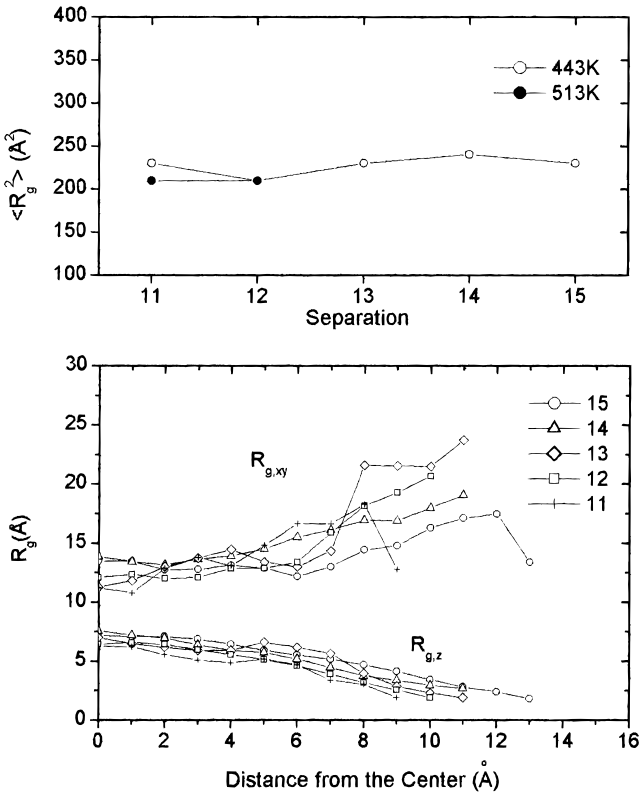

Figure 9. Average of the squared radius of gyration (top) and the parallel component ($R_{g,xy}$) and the perpendicular component ($R_{g,z}$) of the radius of gyration as a function of the distance of the center of mass from the middle of the film.

perpendicular component near the wall is smaller than that of the middle region, which indicates that chains near the walls are flattened and parallel to the wall. At the same position of the chain in the confined system, the perpendicular component decreases with compression. Unlike the linear dependence of the perpendicular component along the distance from the center of the confined system, the parallel component shows a large anisotropy dependence of the chain position along the confined geometry. The chains are expanded in the parallel direction much more near the wall than in the middle of the confined system.

Kumar et al.[1,2] observed the isotropic region in a confined system which starts from $\sim 2R_g$ from the walls, meaning that at least $\sim 4R_g$ size of separation would be required to observe the isotropic middle region. In the very thin confined system which is thinner than $\sim 4R_g$ like our systems, no isotropic region would be expected. The effect of the confinement exists not only in the surface region and but also in the middle region of the very thin confined system.

Along with the change in static properties with compression, the change in the dynamic property has been studied for the center-of-mass diffusion. The parallel component of the center-of-mass diffusion parallel to the wall surface, D_{xy}, and the one perpendicular to the wall surface, D_z, were calculated in units of Å^2/MCS based on the following equations.

$$D_z = \frac{\sum_{i=0}^{N} \{z_{C.M.}(t+i) - z_{C.M.}(0+i)\}^2}{2t(N+1)} \qquad (3)$$

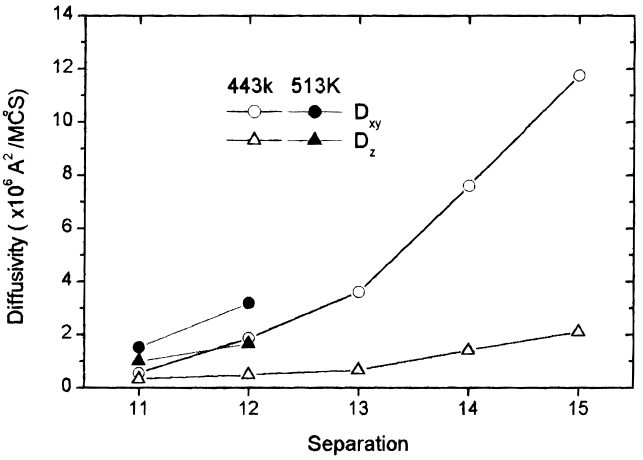

Figure 10. Diffusivity in the parallel direction to the wall surface (D_{xy}) and the perpendicular direction to the wall surface (D_z), evaluated at 3 million Monte Carlo steps.

$$D_{xy} = \frac{\sum_{i=0}^{N}\{[x_{\text{C.M.}}(t+i) - x_{\text{C.M.}}(0+i)]^2 + [y_{\text{C.M.}}(t+i) - y_{\text{C.M.}}(0+i)]^2\}}{4t(N+1)} \quad (4)$$

Here, $N + 1$ denotes the total number of conformations for the ensemble average. With these definitions, D_{xy} approaches a constant positive value as $t \rightarrow \infty$, but D_z approaches zero in the same limit, due to the finite thickness of the film. Six thousand conformations and 3 million Monte Carlo steps were used for N and t.

As shown in Figure 10, the center-of-mass diffusivity of a chain in the direction parallel to the wall surface slows down around 10 times when the polymer melt is compressed from $H = 15$ to $H = 11$. The movement in the direction perpendicular to the wall surface is much slower than the parallel movement with low compression. Shaeffer[5] observed that confinement does not enhance the chain entanglement, and confinement itself is not responsible for the sluggish dynamics in the confined system. However, the entanglement of the chains is expected to increase with compression, due to the increase of the density. At the highest compression, the chains are almost immobilized.

Conclusions

The effect of compression in the very thin confined system whose width is varied from $\sim 3R_g$ to $\sim 2R_g$ with compression has been studied using a Monte Carlo simulation in a high coordination lattice incorporating short-range and long-range interactions. The findings are summarized as follows.

(1) The bead density increases with compression throughout the confined system. The density profile has a stronger oscillation at the higher compression. The temperature change applied in this study has little effect on the density profile. The increase of the bead density at the wall results from the increased trans conformation at the wall providing more efficient packing, while the increase in the middle region is due to the increased gauche conformation, making the chain dimension smaller.

(2) All regions in the confined system are affected by the compression, giving no isotropic region as was found in thicker films from other studies. The effect of compression is intense near the walls, and it is communicated into the middle region of the confined geometry.

(3) The train structure at the wall increases in length and amount with compression. The train of three beads is the most abundant form. However, the bonds of the chain are oriented randomly producing a very low surface ordering. This is an indication that chain ordering at a large scale is hampered in the compressed system, perhaps due to slowing down of chain mobility by compression. Through the temperature dependence of the length of the train structure and the surface ordering, the qualitative agreement with the increase of the crystallization temperature with pressure was observed.

(4) Each component of the chain dimension is a strong function of its location in the compressed system, but the total chain dimension represented by the squared radius of gyration does not vary much with temperature and compression. The parallel component of the chain dimension to the wall tends to decrease as the chain goes to the middle while the perpendicular component shows the reverse tendency.

(5) The chain mobility is suppressed by compression. The diffusivity in the parallel direction to the wall surface is more largely affected by compression than the perpendicular component. The parallel diffusivity is always larger than the perpendicular one.

Acknowledgment. This work was supported by the National Science Foundation (Grants DMR-95-23278 and DMR-98-44069).

References and Notes

(1) Kumar, S. K.; Vacatello, M.; Yoon, D. Y. *J. Chem. Phys.* **1988**, *89*, 5206.
(2) Kumar, S. K.; Vacatello, M.; Yoon, D. Y. *Macromolecules* **1990**, *23*, 2189.
(3) Pakula, T. *J. Chem. Phys.* **1991**, *95*, 4685.
(4) Baschnagel, J.; Binder, K. *Macromolecules* **1995**, *28*, 6808.
(5) Shaeffer, J. S. *Macromolecules* **1996**, *29*, 1010.
(6) Pai-Panandiker, R. S.; Dorgan, J. R.; Pakula, T. *Macromolecules* **1997**, *30*, 6348.
(7) Yoon, D. Y.; Smith, G. D.; Matsuda, T. *J. Chem. Phys.* **1993**, *98*, 10037.
(8) Yoon, D. Y.; Vacatello, M.; Smith, G. D. In *Monte Carlo and Molecular Dynamics Simulations in Polymer Science*; Binder, K., Ed.; Oxford University Press: Oxford, 1995; p 433.
(9) Rapold, R. F.; Mattice, W. L. *J. Chem. Soc., Faraday Trans.* **1995**, *91*, 2435.
(10) Cho, J.; Mattice, W. L. *Macromolecules* **1997**, *30*, 637.
(11) Baschnagel, J.; Binder, K.; Doruker, P.; Gusev, A. A.; Hahn, O.; Kremer, K.; Mattice, W. L.; Müller-Plathe, F.; Murat, M.; Paul, W.; Santos, S.; Suter, U. W.; Tries, V. *Adv. Polym. Sci.*, in press.
(12) Doruker, P.; Mattice, W. L. *Macromolecules* **1998**, *31*, 1418.
(13) Mattice, W. L.; Suter, U. W. *Conformational Theory of Large Molecules. The Rotational Isomeric State Model in Macromolecular Systems*; Wiley: New York, 1994.
(14) Jang, J.; Mattice, W. L. *Polymer* **1999**, *40*, 4685.
(15) Abe, A.; Jernigan, R. L.; Flory, P. J. *J. Am. Chem. Soc.* **1966**, *88*, 631.
(16) Leute, U.; Dollhopf, W.; Liska, E. *Colloid Polym. Sci.* **1976**, *254*, 237.
(17) Doye, J. P. K.; Frenkel, D. *J. Chem. Phys.* **1998**, *109*, 10033.

MA991605M